Research article

Dual-template synthesis of SFO-type aluminophosphate with enhanced water-sorption-driven cooling performance

Qunzheng Jin [a,b,c], Min Xu [a,b,c,*], Zhangli Liu [a,c], Xiulan Huai [a,b,c], Hailiang Wang [d]

[a] Institute of Engineering Thermophysics, Chinese Academy of Sciences, Beijing, 100190, China
[b] Nanjing Institute of Future Energy System, Nanjing, 211135, China
[c] University of Chinese Academy of Sciences, Beijing, 100049, China
[d] Weifang Institute of Technology, Qingzhou, Shandong, 262500, China

ARTICLE INFO

ABSTRACT

Water-based adsorption chillers (ADC) driven by low-grade thermal energy are environment-friendly alternatives to the traditional compression ones to realize the net zero carbon target. Aluminophosphates molecular sieve (AlPOs) is an excellent material for water-based adsorption applications. However, AlPOs suffers from relatively high cost attributed to the extensive use of expensive structure direct agents (SDAs). This study employed a dual-template method, using cheap organic amine as a dual-template, to synthesize low-cost and excellent adsorbent AlPOs with SFO topology (AlPO-SFO). AlPO-SFO synthesized with dual templates shows high crystallinity, large micropore volume, excellent water uptake, and low regeneration temperature. AlPO-SFO guided by 4-dimethylaminopyridine (4-DMAPy) and diethanolamine (DEOA) molar composition of 0.4 and 0.1 exhibits large microporous volume (0.30 ml g^{-1}), high water uptake (0.26 g g^{-1} at $P/P_0 = 0.25$) and low regeneration temperature (65 °C). Importantly, this AlPO-SFO exhibits a high coefficient of performance (COP) of 0.89 for cooling at a low driven temperature of 64 °C. The additive amine providing alkaline medium ensures the practical synthesis of AlPO-SFO when expensive 4-DMAPy decreases, endowing the 42 % reduction of the raw material cost. The results provide a cheaper synthesis route of AlPO-SFO, which is conducive to its large-scale production as a distinguished adsorbent for adsorption chillers.

1. Introduction

Energy demands for heating and cooling account for 51 % of total final energy consumption and more than 40 % of global energy-related carbon dioxide (CO$_2$) emissions [1]. Inside, cooling demands are expected to grow rapidly in future decades because of highly extensive expansions of building areas [2]. For preventing rapidly growing CO$_2$ emissions, a strait global target of net zero by 2050 highlighted the ambition of reducing emissions [3]. Therefore, it is meaningful to seek more low-carbon pathways for the cooling process.

Adsorption chillers, characterized by low-temperature-driven cooling systems using waste heat or solar energy [4–6], have good prospects to withstand the rapidly growing demand for refrigeration. In adsorption chillers, the refrigerant is evaporated and adsorbed onto the internal surfaces of a highly porous solid adsorbent. After the adsorbent is heated, the refrigerant vapor is released and

---

* Corresponding author. Institute of Engineering Thermophysics, Chinese Academy of Sciences, Beijing, 100190, China.
*E-mail address:* xumin@iet.cn (M. Xu).

Table 1
Details of initial gel compositions, synthesis conditions and product structures.

| Samples	Initial molar gel compositions							Temperature(°C)	Time(h)
	Al_2O_3	P_2O_5	HF	4-DMAPy	Dual template type	Dual template ratio	H_2O		
4-DMAPy-1	0.5	0.5	0.25	0.4	/	/	40	175	72
PEG-1	0.5	0.5	0.25	0.4	PEG	0.1	40	175	72
DEOA-1	0.5	0.5	0.25	0.4	DEOA	0.1	40	175	72
TEOA-1	0.5	0.5	0.25	0.4	TEOA	0.1	40	175	72
DEA-1	0.5	0.5	0.25	0.4	DEA	0.1	40	175	72
TEA-1	0.5	0.5	0.25	0.4	TEA	0.1	40	175	72
4-DMAPy-2	0.5	0.5	0.25	0.35	/	/	40	175	72
PEG-2	0.5	0.5	0.25	0.35	PEG	0.15	40	175	72
DEOA-2	0.5	0.5	0.25	0.35	DEOA	0.15	40	175	72
TEOA-2	0.5	0.5	0.25	0.35	TEOA	0.15	40	175	72
DEA-2	0.5	0.5	0.25	0.35	DEA	0.15	40	175	72
TEA-2	0.5	0.5	0.25	0.35	TEA	0.15	40	175	72
4-DMAPy-3	0.5	0.5	0.25	0.3	/	/	40	175	72
PEG-3	0.5	0.5	0.25	0.3	PEG	0.2	40	175	72
DEOA-3	0.5	0.5	0.25	0.3	DEOA	0.2	40	175	72
TEOA-3	0.5	0.5	0.25	0.3	TEOA	0.2	40	175	72
DEA-3	0.5	0.5	0.25	0.3	DEA	0.2	40	175	72
TEA-3	0.5	0.5	0.25	0.3	TEA	0.2	40	175	72
4-DMAPy-4	0.5	0.5	0.25	0.25	/	/	40	175	72
PEG-4	0.5	0.5	0.25	0.25	PEG	0.25	40	175	72
DEOA-4	0.5	0.5	0.25	0.25	DEOA	0.25	40	175	72
TEOA-4	0.5	0.5	0.25	0.25	TEOA	0.25	40	175	72
DEA-4	0.5	0.5	0.25	0.25	DEA	0.25	40	175	72
TEA-4	0.5	0.5	0.25	0.25	TEA	0.25	40	175	72

condensed, meanwhile, heat releases and the adsorbent regenerates. Thus, adsorbent-refrigerant pairs as working mediums play important roles in the performance of adsorption chillers. Adsorbent-refrigerant pairs are divided into physical adsorption working pairs, chemical adsorption working pairs, and composite adsorption working pairs according to the adsorption type [7,8]. Common working pairs include activated carbon (AC)/ammonia, AC/methanol, AC/ethanol, silica gel-water [9], zeolite-water, etc. Water is a ubiquity ideal working fluid avoiding the leakage of hydrofluorocarbon-type refrigerants, which were banned by the European Union legislation (2014) and Paris Accord (2016) [10]. Environment-benign water-sorption-based chillers, driven by low-grade heat, are qualified for raising energy efficiency and reducing energy consumption which is decided by an efficient water adsorbent.

AlPOs molecular sieves are significant materials that assume an open framework structure [11]. SFO-type AlPOs with the accessible pore volume (~20 %) and the diameter of a 12-ring window ~0.7 nm show definite adsorption capacity for methanol, n-Hexane, 2, 2-Dimethylbutane, and mesitylene [12]. Recently, Liu et al. [13] reported that AlPO-SFO exhibits a comparable high water-sorption capacity of 0.28 g g^{-1} at $P/P_0 = 0.2$ and record adsorption-chiller COP of 0.85 at an ultralow driven temperature of 63 °C. Under the working conditions ($T_{ev} = 5$ °C, $T_{con} = 30$ °C, and $T_{des} = 65$ °C), a superior high SCP$_{max}$ of 2.22 kW kg^{-1} and SCP$_{80\%}$ of 1.1 kW kg^{-1} for this material with the particle size of 0.45–0.6 mm is achieved [13]. AlPO-SFO paves a low-carbon way to realize energy-efficient ultra-low-temperature-driven refrigeration. Thus, the excellent application potential of AlPO-SFO urges us to further improve the relevant research of AlPO-SFO, including the optimization of preparation methods, etc.

Synthesis of AlPO needs an Al source, P source, and structure-directing agent (SDA). The SDA of AlPO-SFO, 4-dimethylaminopyridine (4-DMAPy), is a highly efficient agent used in synthesis. However, it costs more than other SDAs and raw materials, which makes AlPO$_4$-SFO hard to promote. Hydrothermal synthesis with a dual-template strategy is a common method for controlling atom distributions [14], changing polymorph type [15], regulating pore diameter [16–19], improving application characteristics [20,21], and enhancing synthesis rate [22–25]. Zhang et al. [26] used tetraethylammonium hydroxide (TEAOH) and morpholine (Mor) as mixed templates to investigate the effects of different template ratios on the physicochemical properties of SAPO-34 molecular sieve. With the increase of Mor, the grains were smooth and regular cubes, meanwhile, the mesoporous content was higher. With the increase of TEAOH, the grain surface gradually changed into a multi-grain stacking structure, and the large-sized mesopores slowly disappeared, replaced by small-sized mesopores with a diameter of 3–4 nm. D. Mishra et al. [22] employed C6 and C12 -surfactants as porogen to control the porous structure of ZSM-5 and successfully obtained ZSM-5 with wider porous structure as a better catalyst on methane into benzene. That proves dual-template mothed is a potential way to decrease cost by replacing expensive SDA with cheap SDA and keeping or strengthening pore characteristics of materials. In this work, a dual-template strategy to hydrothermally synthesize AlPO-SFO with fewer 4-DMAPy was reported. Based on the 4-DMAPy molar composition of 0.5, part of 4-DMAPy was replaced with other agents, such as polyethylene glycol (PEG), diethanolamine (DEOA), triethanolamine (TEOA), diethylamine (DEA) and triethylamine (TEA). We characterized the samples towards X-ray diffraction (XRD), scanning electron microscope (SEM), and water-adsorption application. Via evaluation of water adsorption capacity and max COP of cooling at $T_{ev} = 5$ °C and $T_{con} = 30$ °C, the adsorption abilities of the samples were similar to the original AlPO-SFO. Comparing the raw materials cost between the original AlPO-SFO and the samples synthesized in this work, the dual-template strategy is confirmed cost-effective method to synthesize AlPO-SFO with more than 40 % cost reduction. This work provides a low-cost synthesis way of AlPO-SFO for realizing affordable,
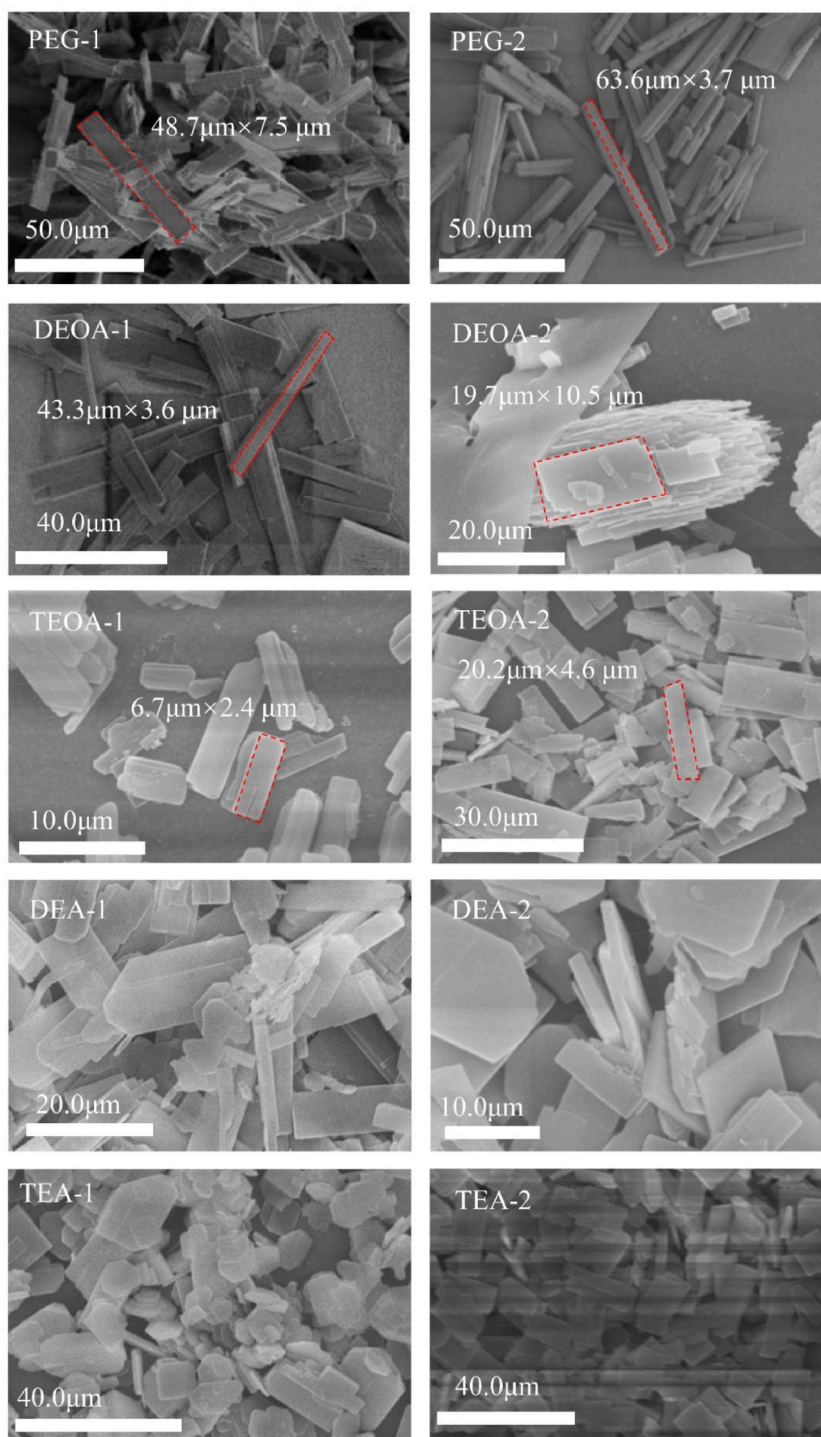
Fig. 1. SEM images of APO-SFO.
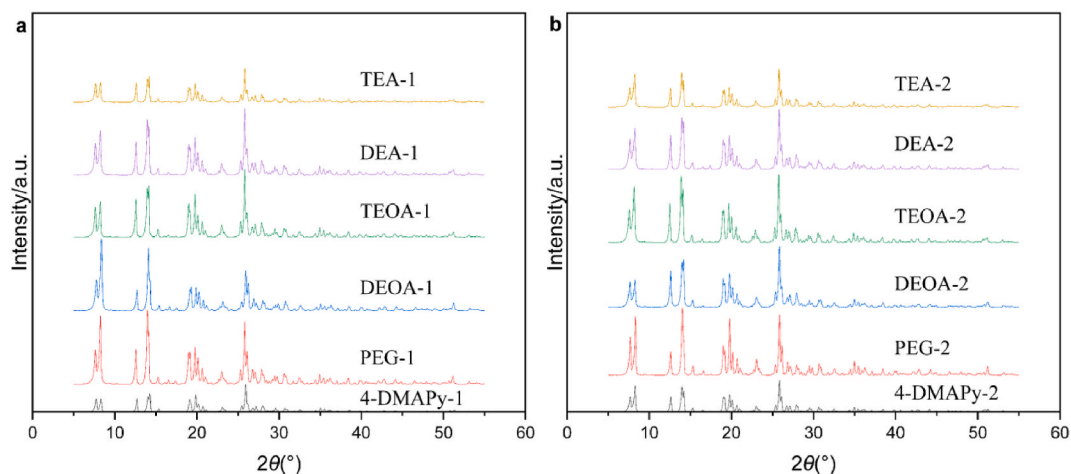
Fig. 2. The XRD patterns of APO-SFO of APO-SFO samples. a. XRD patterns of APO-SFO synthesized with a 4-DMAPy molar composition of 0.4; b. XRD patterns of APO-SFO synthesized with a 4-DMAPy molar composition of 0.35.

scalable, and high-performance adsorption cooling, which is conducive to the promotion of adsorption chillers.

2. Experimental section

2.1. Materials

SFO-type AlPO molecular sieves were traditional hydrothermal synthesized with pseudo-boehmite (AlOOH•nH$_2$O, n = 0.08–0.62), phosphoric acid (H$_3$PO$_4$, 85 wt% in water), hydrofluoric acid (HF, 40 wt% in water) and 4-DMAPy as sources of aluminum, sources of phosphorus, mineralizer, and organic template. The dual templates include PEG (average Mn 600), DEOA (AR, 99.0 %), TEOA (AR, ≥98 %), DEA (ACS), and TEA (AR, 99.0 %). All materials were purchased from Shanghai Macklin Biochemical Co., Ltd and used directly without further purification.

2.2. Hydrothermal synthesis of AlPO-SFO molecular sieves

Table 1 gives the details of initial gel compositions, and synthesis conditions for different samples. The typical synthesis can be described as follows: (1) phosphoric acid was diluted in deionized water; (2) pseudo-boehmite was added to the diluted phosphoric acid solution, followed by strong stirring at room temperature for 10 min to form a homogeneous suspension; (3) the mineralizer HF, organic template 4-DMAPy and dual-template (if needed) were added to the precursors, followed by another 10 min of stirring and 10 min of ultrasonication; (4) the gel was transferred to Teflon-lined stainless-steel autoclave at the required temperature for certain crystallization time; (5) after cooling down to room temperature, the white powder was collected by centrifuged, washed with deionized water, and dried in a vacuum oven; (6) to remove the template, the as-synthesis samples were calcined directly at 600 °C for 6 h with heating rates of 5 °C min^{-1}.
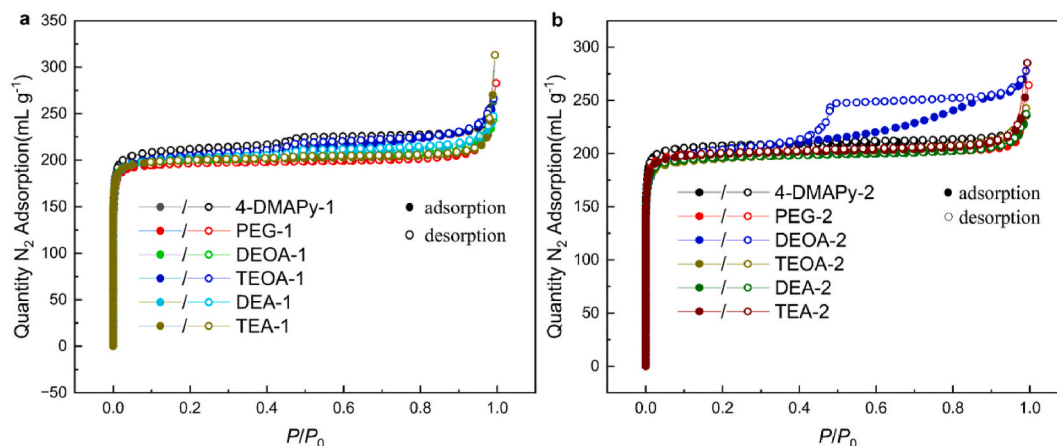
2.3. Characterization

The powder XRD patterns were recorded under ambient conditions at room temperature with a BRUKER instrument (D8 Focus, Cu K$_\alpha$ with k = 1.5418 Å). The morphologies of samples were characterized by SEM (Hitachi S4800). Specific surface area and pore volume of samples were obtained by nitrogen gas adsorption at a low temperature of 77 K using a gas adsorption analyzer (Quantachrome Quadrasorb SI-MP).

Water-sorption analysis was performed by a 3H-2000 PW intelligent gravimetric analyzer (IGA, Beishide Instrument Technology Co., Ltd.). The IGA was automatically operated to precisely control the temperature (30 °C, 40 °C, and 50 °C) and water vapor pressure (1–95 % RH). Before adsorption experiments, samples were completely dehydrated at 150 °C under vacuum to a constant weight.

3. Results and discussion

3.1. Typical characterizations

The samples with different dual-templates synthesized present various morphologies with variable shapes and sizes as shown in Fig. 1. The samples PEG-1, PEG-2, and DEOA-1, represent columnar morphology with similar sizes and uniform shapes, while other samples show flaky morphology with different sizes and shapes, indicating the good crystallinity and high purity of synthesized

4

Fig. 3. The typical characterizations of APO-SFO samples. a. Nitrogen adsorption/desorption isotherms of APO-SFO synthesized with a 4-DMAPy molar composition of 0.4; b. Nitrogen adsorption/desorption isotherms of APO-SFO synthesized with a 4-DMAPy molar composition of 0.35.

Table 2
Pore character of samples.

samples	Total Surface Area (m^2/g)	Micropore Area (m^2/g)	Total Pore Volume (ml/g)	Micropore Volume (ml/g)	Average Pore Diameter(nm)	Average Micropore Diameter(nm)
4-DMAPy-1	855	823	0.41	0.31	1.92	0.60
PEG-1	811	800	0.38	0.30	1.89	0.60
DEOA-1	828	809	0.38	0.30	1.82	0.59
TEOA-1	825	777	0.41	0.30	1.98	0.60
DEA-1	825	801	0.38	0.30	1.85	0.60
TEA-1	824	811	0.44	0.30	2.11	0.59
4-DMAPy-2	857	840	0.36	0.31	1.69	0.59
PEG-2	834	827	0.38	0.31	1.81	0.59
DEOA-2	801	694	0.43	0.26	2.14	0.59
TEOA-2	796	769	0.37	0.29	1.88	0.59
DEA-2	810	798	0.37	0.30	1.80	0.59
TEA-2	821	805	0.41	0.30	1.99	0.58
PEG-3	800	786	0.39	0.30	1.95	0.60
DEOA-3	828	759	0.48	0.30	2.34	0.59
TEOA-3	834	821	0.36	0.31	1.71	0.59
DEA-3	809	794	0.36	0.30	1.76	0.59
TEA-3	830	817	0.40	0.31	1.91	0.60
PEG-4	552	544	0.25	0.20	1.79	0.60
DEOA-4	851	825	0.38	0.32	1.77	0.60
TEOA-4	856	780	0.41	0.30	1.93	0.60
DEA-4	814	802	0.36	0.30	1.76	0.60
TEA-4	849	827	0.37	0.31	1.75	0.59

samples. However, we find zeolite-like crystals have a uniform shape in the ununiform size of length (2–11 μm) and width (6–60 μm), while the original one has a uniform small morphology which is two-edged sword-shaped at 0.1–1 μm scale [13], indicating the deterioration of mass transfer and mechanical properties. Comparing DEOA-1 and DEOA-2, the morphology of the crystals converts to flakiness from columnar with the 4-DMAPy molar composition decreasing. However, the samples synthesized with PEG kept their cuboid columnar morphology when the 4-DMAPy decreased. PEG is beneficial for the growth of AlPO-SFO crystals. It is clear type and ratio of dual templates influence the morphology of the obtained samples. The 4-DMAPy decreasing and dual-template mixing change the morphology of AlPO-SFO because of the crystal nucleus decreasing and alkalinity changing [27,28]. The small crystal sizes such as flakiness and columnar are beneficial for mass transfer characteristics.

XRD patterns of the samples are presented in Fig. 2 and Fig. S1 in Supplementary Information. All samples exhibit distinct characteristic peaks of SFO-type topological structure. The intensities of diffraction peaks for samples synthesized with PEG, DEOA, TEOA, DEA, and TEA are higher than the ones of sample 4-DMAPy when the amount of 4-DMAPy is the same. It depended on the type of dual template. The high intensities of diffraction peaks indicate the dual-template synthesis method can effectively synthesize pure AlPO-SFO with good crystallinity. The narrow widths of the diffraction peaks prove that the samples have small sizes evidenced by Fig. 1. XRD patterns for the samples of 0.25 and 0.3 4-DMAPy molar composition (Fig. S1 in Supplementary Information) show that few
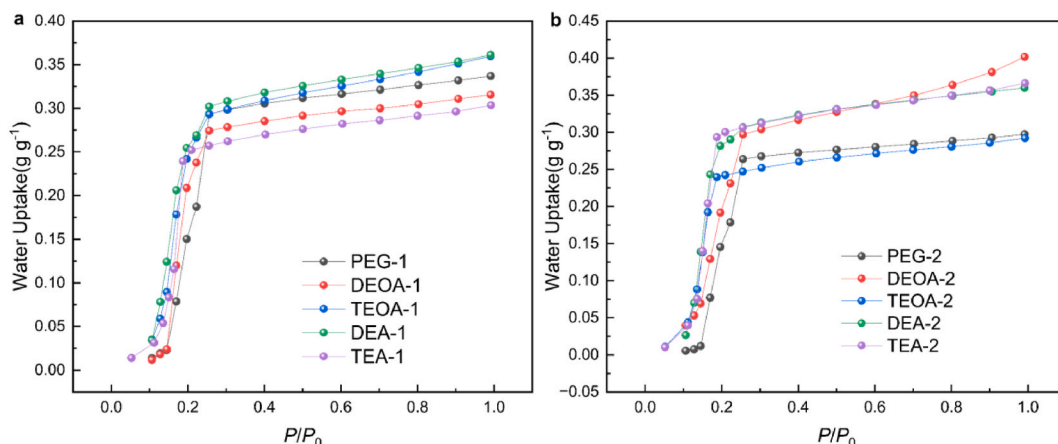
Fig. 4. The curves of water uptake at 30 °C about samples synthesized with a 4-DMAPy molar composition of a. 0.4; b. 0.35.
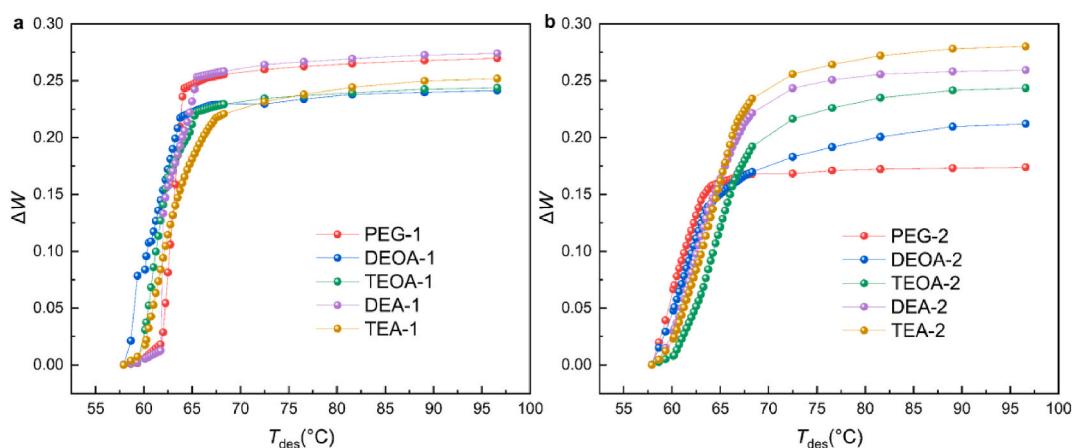
Fig. 5. The thermodynamics calculation of desorption increment. a. Desorption increment curves of samples synthesized with a 4-DMAPy molar composition of 0.4; b. Desorption increment curves of samples synthesized with a 4-DMAPy molar composition of 0.35. Refrigeration conditions used were $T_{ev} = 5$ °C and $T_{con} = 30$ °C.

templates 4-DMAPy will hinder the generation of SFO type topology structures. XRD patterns indicate dual-template approach can successfully synthesize AlPO-SFO with small crystal size and excellent crystallinity.

3.2. Adsorption capacity

N_2 adsorption/desorption isotherms (Fig. 3) show that most of the samples have similar I class sorption curves, indicating the samples possess typical microporous characteristics. However, DEOA-2 has a IVclass sorption curve indicating there are some mesopores. N_2 adsorption/desorption isotherms of 0.25–0.3 4-DMAPy molar composition with dual-template are shown in Fig. S2. Most samples of mole ratio of 0.30 have similar I class curves except DEOA-3. DEOA-3 has IV class sorption curve indicating there are some mesopores like DEOA-2. This proves that DEOA is conducive to the formation of mesopores which is confirmed by the data in Table .2.

The data of the pore character of samples is calculated in the BET method and shown in Table 2. The total surface areas of all samples except PEG-4 are similarly close to 800 m² g⁻¹. The data of micropore area is similar to total surface area which means most pores of samples are micropores except DEOA-2. The micropore area of DEOA-2 is only 694 m² g⁻¹ indicating a poor adsorption capacity. AlPO-SFO synthesized with the assistance of DEOA and PEG exhibit significant differences in pore characteristics. The samples of the DEOA series have a larger pore volume, on the contrary, the pore volume of samples assisted with PEG decreases due to PEG not being able to provide a strongly alkaline environment when the mole ratio of 4-DMAPy is down to 0.25. The samples of 4-DMAPy molar composition of 0.25 except the sample PEG-4 still possess a high micropore volume of 0.29–0.31 ml g⁻¹, while the sample PEG-4 has a poor micropore volume of 0.20 ml g⁻¹. The data in Table .2 indicates that the pore volumes of the materials collapse when the mole ratio of template 4-DMAPy is reduced from 0.3 to 0.25. Overall, the dual-template synthesis method can ensure a good micropore character of AlPO-SFO when the template 4-DMAPy is not too low.

The dual template guided material has good microporous properties, which means that the material has excellent water absorption
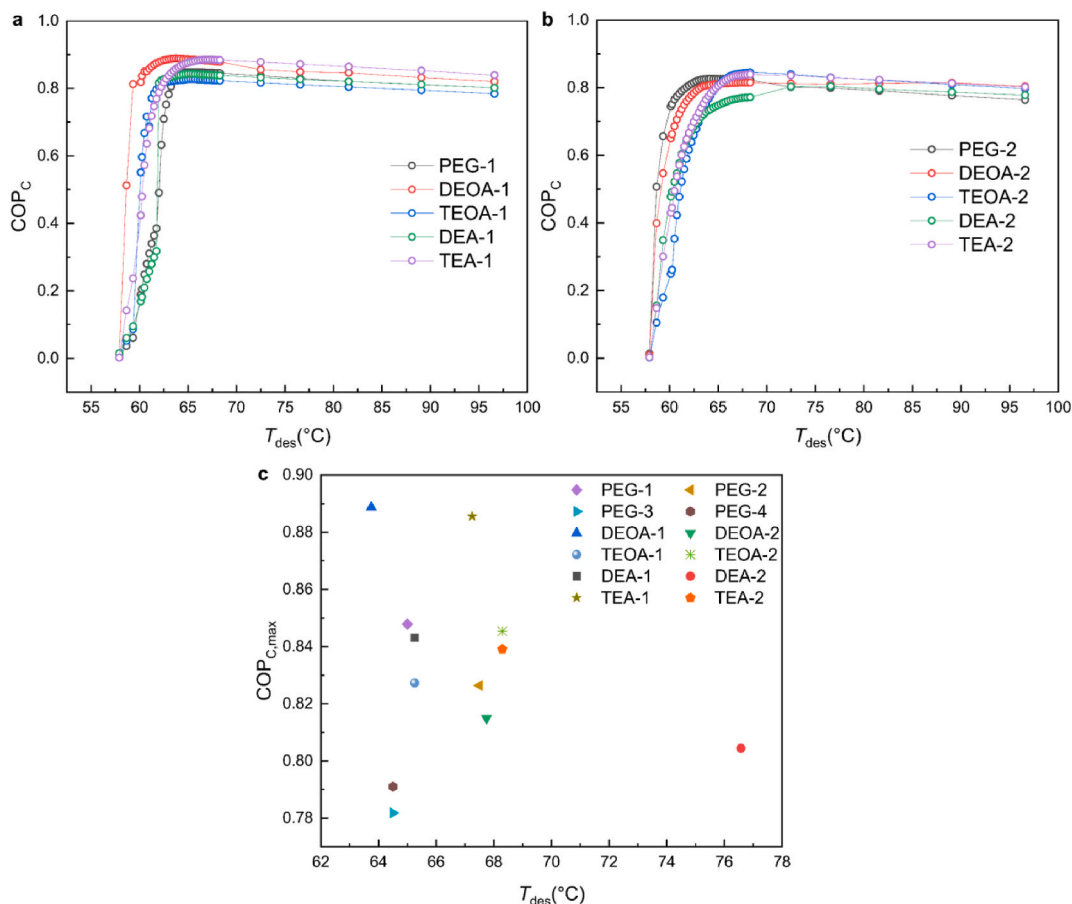
Fig. 6. The thermodynamics calculation of COP. a. COP curves of 0.4 4-DMAPy molar composition samples; b. COP curves of 0.35 4-DMAPy molar composition samples; c. Comparison of maximum COP values and their corresponding driven temperature for cooling of samples. Refrigeration conditions used were $T_{ev} = 5$ °C and $T_{con} = 30$ °C.

performance. It is necessary to conduct water adsorption tests on the above adsorbents. Fig. 4 gives the water adsorption isotherm at 30 °C for the sample assisted with 35–40 %, almost S-shaped, indicating that the materials present excellent water adsorption characteristics. The water adsorption isotherm is similar because they have the same structure type. The water adsorption capacity of samples rapidly increases at $P/P_0 = 0.15$–0.22. Compared to the samples of the 4-DMAPy molar composition of 0.4, the water uptakes of DEOA and TEA rise while the others decrease. The water uptake of sample DEOA-2 increased at $P/P_0 = 0.6$–1.0 attributed to the mesoporous properties of this sample. The water adsorption isotherm of sample DEOA-1 is steepest at $P/P_0 = 0.15$–0.22, such as water uptake of 0.02 g g^{-1} at $P/P_0 = 0.15$ raising to 0.27 g g^{-1} at $P/P_0 = 0.22$, indicating that sample DEOA-1 excellent water adsorption ability. The other samples also show good adsorption capacity. The above analysis proves that the samples synthesized by dual-template have valuable water adsorption capacities suitable for adsorption heat exchangers. The uncertainty of the results for the sorption equilibrium measurements is added in Supplementary Information Note S2.

3.3. ADC performance evaluation

The theoretical COP for cooling and other theoretical parameters based on materials, obtained from the rapid estimation method introduced by de Lange et al. (**Note. S1** in Supplementary Information), is usually used to evaluate the application potential of materials for the adsorption chiller. In this section, we conducted a theoretical evaluation of the thermodynamic properties of these materials.

Fig. 5 shows the variation curves of working capacity for samples with different temperatures, and the cooling conditions are $T_{ev} = 5$ °C and $T_{con} = 30$ °C. For the sample group with the 4-DMAPy molar composition of 0.4 in the initial gel, the cooling workload rapidly increased at the driving heat source temperature of 65 °C, basically exceeding 0.20 g g^{-1} (Fig. 5a). The working capacity of samples assisted by PEG and DEOA exceeded 0.25 g g^{-1}. This indicates that these materials have high energy density at low driving temperatures. When the molar composition of 4-DMAPy is 0.35, the samples gradually achieve high working capacity with the temperature of the driving heat source increasing to ~75 °C (Fig. 5b). The working capacities of PEG-2 and DEOA-2 have significantly

Table 3
Price of raw materials of samples of AlPO-SFO and other potential adsorbent [13].

Sample	Price($/kg)	Price reduction ratio	Sample	Price($/kg)	Price reduction ratio
Origin	85.10	0	PEG-3	42.71	49.80 %
PEG-1	48.68	42.79 %	DEOA-3	43.87	48.44 %
DEOA-1	49.26	42.11 %	TEOA-3	42.39	50.18 %
TEOA-1	48.53	42.97 %	DEA-3	43.16	49.27 %
DEA-1	48.91	42.52 %	TEA-3	44.25	47.99 %
TEA-1	49.46	41.88 %	PEG-4	39.77	53.25 %
PEG-2	45.70	46.30 %	DEOA-4	41.20	51.57 %
DEOA-2	46.56	45.29 %	TEOA-4	39.38	53.72 %
TEOA-2	45.46	46.57 %	DEA-4	40.34	52.58 %
DEA-2	46.19	45.89 %	TEA-4	41.70	50.99 %
TEA-2	46.86	44.93 %	MOF-801	380	
MIP-200	2.02×10^5		MIL-160	879	
AlPO-LTA	8.42×10^4		silica gel	2.79	

decreased to <0.20 g g^{-1}. The above analysis indicates that the molar content of template 4-DMAPy in the initial gel should not be less than 0.35 to ensure the appreciable energy density of these materials.

The average adsorption enthalpies were calculated according to the water adsorption isotherms at three different temperatures (Fig. 4 and Figs. S3a and b) and the Clausius Clapeyron equation, listed in Table S1 in Supplementary Information. The average water adsorption enthalpies (44.65–48.93 kJ mol^{-1}) of samples resemble the original AlPO-SFO (46.76 kJ mol^{-1}) [13], and these values are lower than those of many other benchmarking materials, such as MOF-801 (58.40 kJ mol^{-1}) [26], MIP-200 (51.20 kJ mol^{-1}) [29], MIL-160 (50.64 kJ mol^{-1}) [30], CAU-10 (53.50 kJ mol^{-1}) [31], AlPO-LTA (55.58 kJ mol^{-1}) [32], FAPO-5 (56.10 kJ mol^{-1}) [33] and SAPO-34 (57.00 kJ mol^{-1}) [34]. The ultra-low adsorption enthalpies and perfect S-shaped adsorption isotherms portend extremely high COP$_C$ driven by ultra-low temperatures.

The curves of COPc with driving heat source temperature are shown in Fig. 6a and b, and the cooling conditions are $T_{ev} = 5$ °C, $T_{con} = 30$ °C. which is calculated by the formulas shown in the **Note. S1** [35] in the supplement information. The COPc of the samples rapidly increases at a driving heat source temperature of around 65 °C, reaching the maximum value of 0.8 or even higher. The COPc of the samples with the 4-DMAPy molar composition of 0.4 in the initial gel is slightly higher than those of the samples with a content of 0.35. This indicates that AlPO-SFO synthesized with the assistance of other templates can achieve efficient adsorption heat conversion under ultra-low temperature thermal driving. Fig. 6c shows the optimal COPc and corresponding driving heat source temperatures for these materials. All samples except DEA-2 reach the highest COPc driven by a heat source below 69 °C. The maximum value of COPc is 0.89, which is significantly higher than the original AlPO-SFO (0.85) [11], MOF-801 (0.64) [31], MIP-200 (0.72) [32], MIL-160 (0.76) [33], and AlPO LTA (0.76). It is worth noting that DEOA-1 achieves COPc of 0.89 driven by a highly low-temperature heat source at 64 °C.

The raw materials cost for adsorbents is a key factor in their promotion and application. Table .3 provides the calculation results of raw materials (in lab-scale) cost for synthesized samples in this article. The raw materials cost for AlPO4-SFO synthesized by the original method is 85.10 $ kg-1. The raw materials costs of samples decrease rapidly with the molar ratio of 4-DMAPy decreasing. The raw materials cost of DEOA-1 with excellent ADC performance is 49.26 $ kg-1, which is a lower price for raw materials. Compared to other potential adsorbent, such as MOF-801(380 $ kg-1), MIP-200(2.02 × 105 $ kg-1), MIL-160(880 $ kg-1), AlPO-LTA(8.42 × 104 $ kg-1) [13], there is an obvious advantage in business with AlPO-SFO and DEOA-1. Using the dual-template synthesis method greatly reduces the raw materials cost, which can be reduced by over 40 %. This paper successfully prepared AlPO-SFO adsorbent with excellent pore properties, high coefficient of performance, and low desorption temperature using the dual-template method with low cost of raw materials, promoting the large-scale production of AlPO-SFO.

4. Conclusion

High-purity AlPO-SFO with columnar and flakiness morphology can be obtained by dual template synthesis with the 4-DMAPy molar composition of 0.35–0.4. Significantly, when 4-DMAPy decreased to 30 % or less, the dual template suppressed the purity of AlPO-SFO. Sample DEOA-1, a pure AlPO-SFO synthesized hydrothermally with dual-template shows a high micropore volume of 0.30 ml g^{-1}, perfect S-type water-adsorption isotherm, an excellent water capacity of 0.26 g g^{-1} at $P/P_0 = 0.25$, proving that this material can achieve efficient adsorption heat conversion driven by ultra-low temperature thermal. DEOA-1 shows the highest COP$_C$ of 0.89 at $T_{des} = 64$ °C, $T_{ev} = 5$ °C, and $T_{con} = 30$ °C, indicating that this material holds great potential as an adsorbent used in adsorption chillers. In this paper, the structure direct agent, 4-DMAPy, has been reduced to 40 %, and the raw materials cost is cut down to 58 %. More importantly, the performance of the synthesized sample is similar to the previous ones. The dual-temperature synthesis for AlPO-SFO is a highly efficient and low-cost method for large-scale production.

Data availability

Data will be made available on request.

CRediT authorship contribution statement

Qunzheng Jin: Writing – original draft, Investigation, Formal analysis, Data curation. **Min Xu:** Writing – review & editing, Supervision, Conceptualization. **Zhangli Liu:** Writing – review & editing. **Xiulan Huai:** Supervision, Project administration, Funding acquisition. **Hailiang Wang:** Validation.

Declaration of competing interest

The authors declare that they have no known competing financial interests or personal relationships that could have appeared to influence the work reported in this paper.

Acknowledgments

Appendix A. Supplementary data

Supplementary data to this article can be found online at https://doi.org/10.1016/j.heliyon.2024.e30744.

References

[1] REN21, Renewables 2022 global status report. https://www.unep.org/resources/report/renewables-2022-global-status-report, 2022.
[2] IRENA, IEA and REN21, Renewable energy policies in a time of transition: heating and cooling. https://www.irena.org/publications/2020/Nov/Renewable-Energy-Policies-in-a-Time-of-Transition-Heating-and-Cooling, 2020.
[3] IEA, Net zero by 2050. https://www.iea.org/reports/net-zero-by-2050, 2021.
[4] Q.W. Pan, R.Z. Wang, Sol. Energy 172 (2018) 24–31.
[5] M. Pons, F. Poyelle, Int. J. Refrig. 22 (1999) 27–37.
[6] P.R. Chauhan, S.C. Kaushik, S.K. Tyagi, Renew. Sustain. Energy Rev. 154 (2022) 111808.
[7] Ahmed A. Askalany, M. Salem, I.M. Ismael, A.H.H. Ali, M.G. Morsy, BidyutB. Saha, Renew. Sustain. Energy Rev. 19 (2013) 565–572.
[8] L. Jiang, L.W. Wang, W.L. Luo, R.Z. Wang, Renew. Energy 74 (2015) 287–297.
[9] Q.W. Pan, R.Z. Wang, Sol. Energy 172 (2018) 24–31.
[10] N. Abas, A.R. Kalair, N. Khan, A. Haider, Z. Saleem, M.S. Saleem, Energy Rev. 90 (2018) 557–569.
[11] Kenneth J.D. MacKenzie, Mark E. Smith, Pergamon Materials Series. 6 (2002) 399–457, https://doi.org/10.1016/S1470-1804(02)80008-6.
[12] G. Cao, M.J. Shah, D.L. Dorset, K.G. Strohmaier, J.F. Brody, R. Xu, Z. Gao, J. Chen, W. Yan, Studies in surface science and catalysis 170 (2007) 311–313.
[13] Z. Liu, J. Xu, M. Xu, C. Huang, R. Wang, T. Li, X. Huai, Nat. Commun. 13 (2022) 193.
[14] N. Tsunoji, K. Tsuchiya, N. Nakazawa, S. Inagaki, Y. Kubota, T. Nishitoba, T. Yokoi, T. Ohnishi, M. Ogura, M. Sadakane, T. Sano, Multiple templating strategy for the control of aluminum and phosphorus distributions in AFX zeolite, Microporous and Mesoporous Mater. 321 (2021) 111124.
[15] T. Lu, R. Xu, W. Yan, Microporous Mesoporous Mater. 226 (2016) 19–24.
[16] N.H. Nguyen, N. Truong-Thi, D.T.D. Nguyen, Y.C. Ching, N.T. Huynh, D.H. Nguyen, Colloids Surf. A Physicochem. Eng. Asp. 655 (2022) 130218.
[17] S. Song, J. Liang, W. Xiao, D. Gu, Chin. Chem. Lett. (2022) 107777.
[18] M. Zhang, Y. Sun, R. Song, Microporous Mesoporous Mater. 330 (2022) 111593.
[19] M. Wang, X. Wang, Q. You, Y. Wu, X. Yang, H. Chen, B. Liu, Q. Hao, J. Zhang, X. Ma, Microporous Mesoporous Mater. 323 (2021) 111207.
[20] N. Xu, Z. Liu, Y. Zhang, H. Qiu, L. Kong, X. Tang, D. Meng, X. Kong, M. Wang, Y. Zhang, Microporous Mesoporous Mater. 298 (2020) 110091.
[21] W. Jiao, J. Su, H. Zhou, S. Liu, C. Liu, L. Zhang, Y. Wang, W. Yang, Microporous Mesoporous Mater. 306 (2020) 110444.
[22] D. Mishra, A. Modak, K.K. Pant, X.S. Zhao, Microporous Mesoporous Mater. 344 (2022) 112172.
[23] Y. Tu, T. Zhan, T. Wu, F. Zhang, I. Kumakiri, X. Chen, H. Kita, Microporous Mesoporous Mater. 327 (2021) 111436.
[24] L. Sun, W. Zhang, Z. Li, M. Yang, Y. Wang, X. Zhang, P. Tian, Z. Liu, Microporous Mesoporous Mater. 315 (2021) 110915.
[25] Z. Liu, Y. Hua, J. Wang, X. Dong, Q. Tian, Y. Han, Mater. Chem. Front. (2017), https://doi.org/10.1039/C7QM00168A.
[26] M.V. Solovyeva, L.G. Gordeeva, T.A. Krieger, Y.I. Aristov, Energy Convers. Manag. 174 (2018) 356–363.
[27] M. Osacký, H. Pálková, P. Hudec, A. Czímerová, D. Galusková, M. Vítková, Microporous Mesoporous Mater. 294 (2020) 109852.
[28] M. Khatamian, M. Saket Oskoui, M. Darbandi, Microporous Mesoporous Mater. 182 (2013) 50–61.
[29] S. Wang, J.S. Lee, M. Wahiduzzaman, J. Park, M. Muschi, C.M. Corcos, A. Tissot, K.H. Cho, J. Marrot, W. Shepard, G. Maurin, J.S. Chang, C. Serre, Nat. Energy 3 (2018) 985–993.
[30] A. Cadiau, J.S. Lee, D.D. Borges, P. Fabry, T. Devic, M.T. Wharmby, C. Martineau, D. Foucher, F. Taulelle, C.H. Jun, Y.K. Hwang, N. Stock, M.F. de Lange, F. Kapteijn, J. Gascon, G. Maurin, J.S. Chang, C. Serre, Adv. Mater. 27 (2015) 4775–4780.
[31] H. Reinsch, M.A. van der Veen, B. Gil, B. Marszalek, T. Verbiest, D.E. de Vos, N. Stock, Chem. Mater. 25 (2013) 17–26.
[32] A. Krajnc, J. Varlec, M. Mazaj, A. Ristić, N.Z. Logar, G. Mali, Adv. Energy Mater. 7 (2017) 1601815.
[33] Y.D. Kim, K. Thu, K.C. Ng, Desalination 344 (2014) 350–356.
[34] L. Zhou, J. Guan, C. Yu, B. Huang, Catalysts 11 (2021) 314.
[35] T.J. Matemb Ma Ntep, M. Wahiduzzaman, E. Laurenz, I. Cornu, G. Mouchaham, I. Dovgaliuk, S. Nandi, K. Knop, C. Jansen, F. Nouar, P. Florian, G. Füldner, G. Maurin, C. Janiak, C. Serre, Adv. Mater. (2023) 2211302.